Predicting the High-Pressure Phase Equilibria of Methane + *n*-Hexane Using the SAFT-VR Approach

Clare McCabe,[†] Alejandro Gil-Villegas,[†,‡] and George Jackson*[,†]

Department of Chemistry, University of Sheffield, Sheffield, S3 7HF, United Kingdom, and Instituto de Física, Universidad de Guanajuato, León 37150, México

Received: November 25, 1997; In Final Form: March 12, 1998

In a recent paper we predicted the fluid-phase equilibria of *n*-butane + *n*-alkane binary mixtures using the statistical associating fluid theory for chain molecules with attractive potentials of variable range (SAFT-VR). Now we focus on the methane + *n*-hexane system, again using the SAFT-VR approach. The methane + *n*-hexane system exhibits type V phase behavior, in which partial miscibility of the two components is observed. The phase diagram for the binary mixture is predicted, and we concentrate on the critical region and liquid−liquid immiscibility observed in this system. The upper and lower critical end-points predicted by the SAFT-VR approach are in excellent agreement with the experimental data, as is the theoretical gas−liquid critical line. We treat the *n*-alkane molecules as chains of united-atom hard-sphere segments with square-well potentials of variable range to describe the attractive interactions. A simple empirical relationship exists between the number of carbon atoms in the alkane molecule and the number of segments in the chain model. The pure component vapor pressure curves and saturated liquid densities are calculated by fitting to experimental data from the triple to the critical point. The optimized parameters are then rescaled to the respective critical points. We use the Lorentz−Berthelot combining rules for the unlike size and energy interactions. It is particularly gratifying to see that type V behavior can be predicted for the methane + *n*-hexane system simply by using Lorentz−Berthelot combining rules.

Introduction

Studies on the partial miscibility of light hydrocarbons with heavier components provide data that are essential in the design of industrial separation processes. It is well-known that the mutual solubility of two components increases with temperature due to entropic dominance of the system's energetic interactions. In such a system the two components are completely miscible, forming a single phase above the upper critical solution temperature (UCST). Systems exist in which the solubility of two components can increase as the temperature decreases, being completely miscible below a lower critical solution temperature (LCST). This behavior often involves hydrogen bonding, and water is generally one of the components. It was realized, however that systems in which hydrogen bonding between the molecules is not a feature could display LCSTs when one of the components is polar.[1] The immiscibility is confined to a short temperature range close to the critical point of the more volatile component; for example, ethane and ethanol show liquid−liquid immiscibility over a small temperature range above the LCST near the critical point of pure ethane.[2] This type of immiscibility is not confined to mixtures with one or two polar components, but can be found in mixtures of nonpolar molecules of the same chemical type providing the molecular sizes and energies of interaction of the two components are significantly different. For example LCSTs are found in mixtures of substances belonging to a particular homologous series when the size difference between the two components exceeds a certain ratio.[1] For mixtures of the *n*-alkanes with methane such liquid−liquid immiscibility is first observed for *n*-hexane close to the critical point of pure methane.

The methane + *n*-hexane system was studied experimentally in the early 1930s and 1940s,[3−6] but there was little information about the composition of the coexisting phases. In 1962 Shim and Kohn[7] determined vapor−liquid equilibrium data for the methane + *n*-hexane system that confirmed the previously reported data, but again they saw no liquid−liquid immiscibility. They did note however a decrease in methane solubility in the liquid phase as the molecular weight of the heavier hydrocarbon increased, concluding that hexane would be the highest hydrocarbon homologue to be completely miscible in methane. Poston and McKetta[8] have published vapor−liquid equilibrium data for five isotherms, with compositions near the critical state being determined for the first time, but at temperatures far removed from the critical point of pure methane, so that no liquid−liquid immiscibility was observed. The situation was clarified by Rowlinson and Davenport,[9] who investigated the solubility of higher hydrocarbons in liquid methane and found hexane to be the first hydrocarbon to show partial miscibility in liquid methane. A full experimental picture of the phase behavior of methane + *n*-hexane was provided by Kobayashi and co-workers.[10,11]

The types of phase diagram exhibited by binary alkane mixtures will be discussed within the classification of Scott and van Konynenburg.[12,13] Simple type I phase behavior involves a continuous gas−liquid critical line connecting the critical points of the two pure components; this type of phase behavior is observed for the methane + *n*-alkane binary mixtures up to and including pentane. The mixture of methane + *n*-hexane exhibits type V behavior. Now a critical line extends from the critical point of the less volatile component, *n*-hexane, to the

[†] University of Sheffield.
[‡] Universidad de Guanajuato.

S1089-5647(98)00335-6 CCC: $15.00
Published on Web 05/06/1998

lower critical end point (LCEP), where it connects to the three-phase line. The three-phase line extends to higher temperatures and pressures terminating at the upper critical end point (UCEP), where a short gas−liquid critical line connects the UCEP to the critical point of the more volatile component, methane. As we move to the next member in the homologous series, solid phases intervene at low temperatures. From the experimental phase diagram[14] it it is not possible to tell if the system would show type V or III phase behavior, as the critical line is hidden.

We have already examined the critical lines for binary mixtures of *n*-alkanes which exhibit type I phase behavior[15] using the SAFT-VR approach.[16,17] Here we examine the binary mixture of methane + *n*-hexane using the SAFT-VR theory. In the original SAFT equations[18] the molecules are treated as chains formed from Lennard-Jones segments, and this approach has been used extensively to examine fluid-phase equilibria (see ref 19 for a recent overview). A simpler version of the theory (SAFT-HS) where the molecules are considered as chains of hard-sphere segments and the attractive interactions are treated at the mean-field level of van der Waals has also been used with some success for aqueous solutions of *n*-alkanes[19] and for mixtures containing hydrogen fluoride.[20] However, while providing a good description of strongly associated systems in which the association interactions dominate the phase behavior, a more precise description of the dispersion forces is necessary for an accurate representation of binary mixtures of *n*-alkanes. With the SAFT-VR approach we achieve this through attractive interactions of variable range. The molecules are treated as chains of square-well segments, the interactions being described by a square-well potential of width λ and depth ϵ.

Models and Theory

The *n*-alkane molecules are modeled by a simple united-atom approach: *m* hard-spherical segments of diameter σ tangentially bonded together to form chains. The interactions are described via square-well potentials of variable range λ_{ij} and depth ϵ_{ij},

$$u_{ij}(r) = \begin{cases} +\infty & \text{if } r < \sigma_{ij} \\ -\epsilon_{ij} & \text{if } \sigma_{ij} \le r < \lambda_{ij}\sigma_{ij} \\ 0 & \text{if } r \ge \lambda_{ij}\sigma_{ij} \end{cases} \tag{1}$$

where r is the distance between the two particles and σ_{ij} defines the contact distance between spheres. A simple empirical relationship between the number of carbon atoms C in the alkyl chain and the number of spherical segments m was proposed in earlier work;[19,21,22] $m = 1 + (C - 1)/3$. Values of $m_1 = 1$ and $m_2 = 2.67$ are hence used for methane and *n*-hexane, respectively.

Here we will summarize only the main expressions of the SAFT-VR approach for the square-well potential; the reader is directed to the previous papers[16,17] for full details. The general equation for mixtures of chain molecules formed from hard-core segments with attractive interactions is given, followed by the expressions for the specific case of interest, i.e., our binary mixture. We should note the contribution due to association is not included for *n*-alkane systems since we are dealing with a nonassociating system. The Helmholtz free energy A for an *n*-component mixture of chain molecules can be separated into the various contributions as[16,17]

$$\frac{A}{NkT} = \frac{A^{\text{IDEAL}}}{NkT} + \frac{A^{\text{MONO}}}{NkT} + \frac{A^{\text{CHAIN}}}{NkT} \tag{2}$$

where N is the total number of molecules, k is the Boltzmann constant, and T is the temperature. The ideal contribution to the free energy is given by a sum over all species i in the mixture,[23]

$$\begin{aligned} \frac{A^{\text{IDEAL}}}{NkT} &= \left(\sum_{i=1}^{n} x_i \ln \rho_i \Lambda_i^3\right) - 1 \\ &= x_1 \ln \rho_1 \Lambda_1^3 + x_2 \ln \rho_2 \Lambda_2^3 - 1 \end{aligned} \tag{3}$$

where $x_i = N_i/N$ is the mole fraction, $\rho_i = N_i/V$ the molecular number density, N_i the number of molecules, and Λ_i the thermal de Broglie wavelength of species i, and V is the volume of the system. We can express the monomer Helmholtz free energy by

$$\begin{aligned} \frac{A^{\text{MONO}}}{NkT} &= \left(\sum_{i=1} x_i m_i\right) \frac{A^{\text{M}}}{N_s kT} \\ &= \left(\sum_{i=1} x_i m_i\right) a^{\text{M}} \\ &= (x_1 m_1 + x_2 m_2) a^{\text{M}} \end{aligned} \tag{4}$$

where m_i is the number of spherical segments of chain i, and N_s is the total number of segments.

Using the Barker and Henderson perturbation theory[24] for mixtures with a hard-sphere reference system, the monomer free energy per segment of the mixture is obtained from the expansion

$$a^{\text{M}} = a^{\text{HS}} + \beta a_1 + \beta^2 a_2 + \ldots \tag{5}$$

where $\beta = 1/kT$ and each term is now for a mixture of spherical segments. The expression of Boublík[25] and Mansoori et al.[26] for a multicomponent mixture of hard spheres is used for the reference hard-sphere term,

$$a^{\text{HS}} = \frac{6}{\pi\rho_s}\left[\left(\frac{\zeta_2^3}{\zeta_3^2} - \zeta_0\right)\ln(1-\zeta_3) + \frac{3\zeta_1\zeta_2}{(1-\zeta_3)} + \frac{\zeta_2^3}{\zeta_3(1-\zeta_3)^2}\right] \tag{6}$$

where $\rho_s = N_s/V$ is the total number density of spherical segments and ζ_l are the reduced densities defined by

$$\begin{aligned} \zeta_l &= \frac{\pi\rho_s}{6}\left[\sum_{i=1}^{n} x_{s,i}\sigma_{ii}^l\right] \\ &= \frac{\pi\rho_s}{6}\left[x_{s,1}\sigma_{11}^l + x_{s,2}\sigma_{22}^l\right] \end{aligned} \tag{7}$$

Here, σ_{ii} is the diameter of the spherical segments of chain i, and $x_{s,i}$ is the mole fraction of segments of type i in the mixture. For the evaluation of the perturbative terms a_1 and a_2 we have used the one-fluid approximation (see ref 17 for more details).

The mean-attractive energy represented by the a_1 term is obtained from the sum of the partial terms corresponding to each type of pair interaction,[16,17]

$$\begin{aligned} a_1 &= \sum_{i=1}^{n}\sum_{j=1}^{n} x_{s,i} x_{s,j} a_1^{ij} \\ &= x_{s,1}^2\, a_1^{11} + 2x_{s,1}x_{s,2}a_1^{12} + x_{s,2}^2\, a_1^{22} \end{aligned} \tag{8}$$

where

$$a_1^{ij} = -2\pi\rho_s\epsilon_{ij}\int_{\sigma_{ij}}^{\infty} r_{ij}^2\, g_{ij}^{HS}[r_{ij};\zeta_{ij}]\, dr_{ij} \tag{9}$$

and g_{ij}^{HS} is the radial distribution function for a mixture of hard spheres. Using the mean value theorem,[16] we obtain an expression for a_1 in terms of the contact value of g_{ij}^{HS}:

$$a_1 = -\rho_s \sum_i \sum_j x_{s,i}x_{s,j}\, \alpha_{ij}^{VDW}\, g_{ij}^{HS}[\sigma_{ij};\zeta_3^{eff}] \tag{10}$$

where

$$\alpha_{ij}^{VDW} = 2\pi\epsilon_{ij}\,\sigma_{ij}^3(\lambda_{ij}^3 - 1)/3 \tag{11}$$

is the van der Waals attractive constant for the $i-j$ interaction, and ζ_3^{eff} is an effective packing fraction.

In the van der Waals one (VDW-1) fluid theory g_{ij}^{HS} is approximated by the radial distribution function for a single fluid so that eq 10 simpifies to

$$a_1 = -\rho_s \sum_i \sum_j x_{s,i}x_{s,j}\, \alpha_{ij}^{VDW}\, g_0^{HS}[\sigma_x;\zeta_x^{eff}] \tag{12}$$

The VDW-1 fluid parameter is given by

$$\sigma_x^{\,3} = \sum_i \sum_j x_{s,i}x_{s,j}\,\sigma_{ij}^3 \tag{13}$$

and g_0^{HS} is the contact value of the hard-sphere pair radial distribution obtained from the Carnahan and Starling equation of state,[27]

$$g_0^{HS}[\sigma_x;\zeta_x^{eff}] = \frac{1 - \zeta_x^{eff}/2}{(1 - \zeta_x^{eff})^3} \tag{14}$$

The effective packing fraction ζ_x^{eff} in eq 14 is obtained, within the VDW-1 fluid approximation, from the corresponding packing fraction of the mixture ζ_x:

$$\zeta_x^{eff}(\zeta_x,\lambda) = c_1(\lambda_{ij})\zeta_x + c_2(\lambda_{ij})\zeta_x^{\,2} + c_3(\lambda_{ij})\zeta_x^{\,3} \tag{15}$$

where

$$\zeta_x = \frac{\pi}{6}\rho_s \sum_i \sum_j x_{s,i}x_{s,j}\,\sigma_{ij}^3 = \frac{\pi}{6}\rho_s\sigma_x^{\,3} \tag{16}$$

and the coefficients c_1, c_2, and c_3 are approximated by those of the pure fluid,[16,17]

$$\begin{pmatrix} c_1 \\ c_2 \\ c_3 \end{pmatrix} = \begin{pmatrix} 2.25855 & -1.50349 & 0.249434 \\ -0.669270 & 1.40049 & -0.827739 \\ 10.1576 & -15.0427 & 5.30827 \end{pmatrix} \begin{pmatrix} 1 \\ \lambda \\ \lambda_2 \end{pmatrix} \tag{17}$$

This corresponds to the MX1b mixing rule of ref 17.

The first fluctuation term a_2 is given by[16,17]

$$a_2 = \sum_{i=1}^{n}\sum_{j=1}^{n} x_{s,i}x_{s,j}\, a_2^{ij} = x_{s,1}^2\, a_2^{11} + 2x_{s,1}x_{s,2}a_2^{12} + x_{s,2}^2\, a_2^{22} \tag{18}$$

The terms a_2^{ij} are obtained with the local compressibility approximation,

$$a_2^{ij} = \frac{1}{2}K^{HS}\epsilon_{ij}\rho_s\frac{\partial a_1^{ij}}{\partial\rho_s} \tag{19}$$

where K^{HS} is the hard-sphere isothermal compressibility of Percus−Yevick,[16]

$$K^{HS} = \frac{\zeta_0(1-\zeta_3)^4}{\zeta_0(1-\zeta_3)^2 + 6\zeta_1\zeta_2(1-\zeta_3) + 9\zeta_2^{\,3}} \tag{20}$$

Finally, the contribution to the free energy due to chain formation is expressed in terms of the contact value of the background correlation function,[16,17]

$$\frac{A^{CHAIN}}{NkT} = -\sum_{i=1}^{n} x_i(m_i - 1)\ln y_{ii}^{SW}(\sigma_{ii}) = -x_1(m_1 - 1)\ln y_{11}^{SW}(\sigma_{11}) - x_2(m_2 - 1)\ln y_{22}^{SW}(\sigma_{22}) \tag{21}$$

where $y_{ii}^{SW}(\sigma_{ii}) = g_{ii}^{SW}(\sigma_{ii})\exp(-\beta\epsilon_{ii})$. We obtain $y_{ii}^{SW}(\sigma_{ii})$ from the high-temperature expansion of $g_{ii}^{SW}(\sigma_{ii})$,

$$g_{ii}^{SW}(\sigma_{ii}) = g_{ii}^{HS}(\sigma_{ii}) + \beta\epsilon_{ii}g_1(\sigma_{ii}) \tag{22}$$

The hard-sphere term g_{ii}^{HS} is given by the expression of Boublík,[25]

$$g_{ij}^{HS}(\sigma_{ij};\zeta_3) = \frac{1}{1-\zeta_3} + 3\frac{D_{ij}\zeta_3}{(1-\zeta_3)^2} + 2\frac{(D_{ij}\zeta_3)^2}{(1-\zeta_3)^3} \tag{23}$$

with the parameter D_{ij} defined by

$$D_{ij} = \frac{\sigma_{ii}\sigma_{jj}\sum_{i=1}^{n} x_{s,i}\sigma_{ii}^2}{(\sigma_{ii} + \sigma_{jj})\sum_{i=1}^{n} x_{s,i}\sigma_{ii}^3} \tag{24}$$

The term $g_1(\sigma_{ii})$ is obtained from a self-consistent method for the pressure p from the Clausius virial theorem and from the density derivative of the Helmholtz free energy,[16,17]

$$g_1(\sigma_{ii};\zeta_3) = g_0^{HS}[\sigma_x;\zeta_x^{eff}] + (\lambda_{ii}^3 - 1)\frac{\partial g_0^{HS}[\sigma_x;\zeta_x^{eff}]}{\partial\zeta_x^{eff}}\left(\frac{\lambda_{ii}}{3}\frac{\partial\zeta_x^{eff}}{\partial\lambda_{ii}} - \zeta_3\frac{\partial\zeta_x^{eff}}{\partial\zeta_3}\right) \tag{25}$$

In our earlier paper[15] for binary mixtures of *n*-alkanes we used the actual packing fraction ζ_3 of the system in order to get ζ_3^{eff} according to the mapping rule for pure components[16] (MX3b mixing rule in ref 17). Although the MX3b mixing rule is the simplest and probably the most accurate representation, there are some problems associated with the critical region of the phase diagram when this mixing rule is used. This is a common feature of equations of state for mixtures that use parameters defined for pure fluids beyond the VDW-1 fluid approximation.[13,28] If one is interested in phase equilibria away from the critical region, the MX3b rule will be the most suitable. However for high-pressure studies of the critical behavior as we present here, the VDW-1 fluid mixing rule MX1b[17] is the

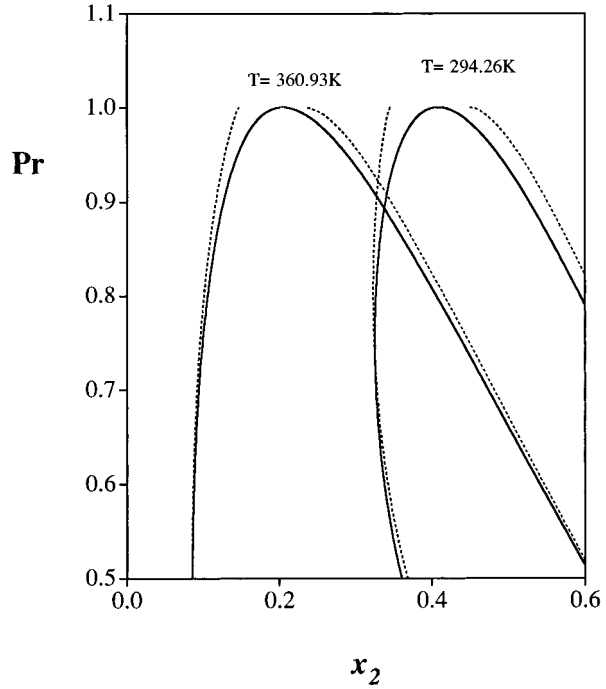

Figure 1. *px* slices at 294.26 and 360.93 K obtained using the two different mixing rules. The continuous curve corresponds to MX1b and the dashed curve to MX3b. The reduced pressure is defined as $Pr = p/p_{UCEP}$ where p_{UCEP} is the pressure of the UCEP.

more appropriate choice. The MX1b prescription gives an excellent representation of both vapor−liquid and liquid−liquid critical behavior, as illustrated in Figure 1, where we show *px* slices at two constant temperatures for the methane + *n*-hexane system obtained using the MX1b and MX3b mixing rules. The inadequacy of the MX3b rule close to the critical temperature is apparent from the figure.

Results and Discussion

Before studying the mixture, the parameters of the potential models for the pure substances have to be determined. Theoretical predictions are fitted to the experimental phase equilibrium data from the triple to the critical point using a simplex method.[29] The optimized pure component size, σ, and energy, ϵ, parameters obtained are then rescaled by their respective experimental critical points since our main interest is in the area around the critical region of the methane + *n*-hexane system. The final values obtained for the hard-sphere diameter and depth of the potential well for methane are $\sigma_1 = 4.100$ Å and $\epsilon_1/k = 161.2$ K, and for hexane $\sigma_2 = 4.497$ Å and $\epsilon_2/k = 244.8$ K. As in our previous paper,[15] we obtain the range parameter λ from a linear relation with the carbon number C ($\lambda = 0.02119C + 1.410$) giving values of $\lambda_1 = 1.431$ for methane and $\lambda_2 = 1.536$ for *n*-hexane. In Figure 2 we compare the vapor pressures for methane and *n*-hexane obtained from the SAFT-VR predictions (rescaled to the critical point) with the experimental data.[30] The rescaled parameters clearly provide a good representation of the vapor−pressure curves for both systems. The calculation of phase equilibria in mixtures requires the determination of a number of unlike parameters obtained from the pure component parameters. The unlike size and energy parameters are obtained using the Lorentz−Berthelot combining rules,[13]

$$\sigma_{ij} = \frac{\sigma_{ii} + \sigma_{jj}}{2} \tag{26}$$

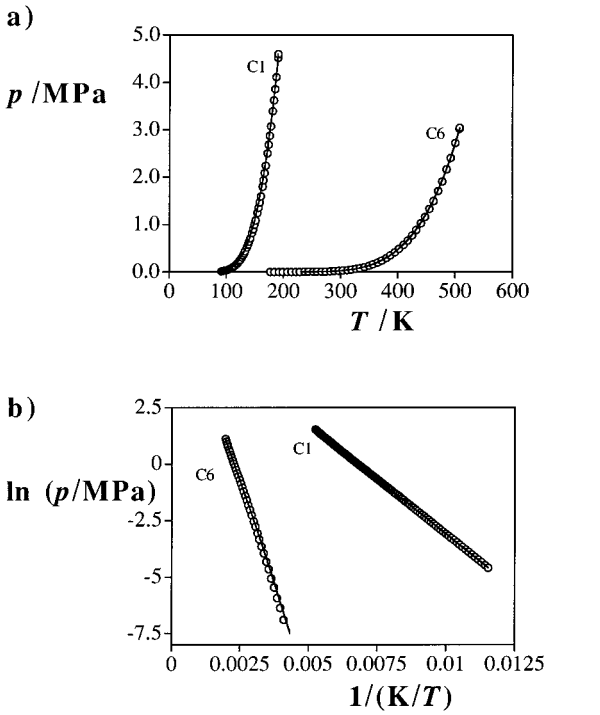

Figure 2. Vapor pressures for methane and *n*-hexane compared with the SAFT-VR predictions. The circles represent the experimental data.[30] The continuous curves represent the SAFT-VR predictions. In a we show the vapor-pressure curve as a *pT* representation, and in b as a Clausius−Clapeyron plot.

$$\epsilon_{ij} = \sqrt{\epsilon_{ii}\epsilon_{jj}} \tag{27}$$

giving $\sigma_{12} = 4.299$ Å and $\epsilon_{12}/k = 198.6$ K. The unlike range parameter is determined from the arithmetic mean,

$$\lambda_{ij} = \frac{\lambda_{ii}\sigma_{ii} + \lambda_{jj}\sigma_{jj}}{\sigma_{ii} + \sigma_{jj}} \tag{28}$$

so that $\lambda_{12} = 1.486$. The predicted *pT* projection of the phase diagram for the methane + *n*-hexane system is compared directly with experimental *pT* data in Figure 3. As discussed earlier, the system shows type V phase behavior with two critical lines. The critical line running from the critical point of the less volatile component, *n*-hexane, to the LCEP changes continuously in character from gas−liquid type to liquid−liquid. A short three-phase line extends from the LCEP to higher pressures and temperatures terminating at the UCEP, which connects to the critical point of the more volatile component, methane, through a second but shorter gas−liquid critical line. This limited region of liquid−liquid immiscibility, which can be seen more clearly in the inset of Figure 3, is described very well by the SAFT-VR approach. The values in the literature for the LCEP and the UCEP are 182.46 K and 3.46 MPa, and 195.91 K and 5.21 MPa, respectively.[11] The theoretical values obtained from SAFT-VR for a square-well potential compare very favorably with the experimental data. We predict 181.31 K and 3.40 MPa for the LCEP, and 193.66 K and 4.92 MPa for the UCEP. To our knowledge there is no experimental data available for the short gas−liquid critical line, and only a few points on the high-pressure critical line have been published. Although there is some discrepancy between the available data, the SAFT-VR predictions are very good: the maximum in the critical line is at 21.0 MPa and 333 K, which is slightly higher in temperature and pressure than the experimental value of 20.8 MPa and 332 K.

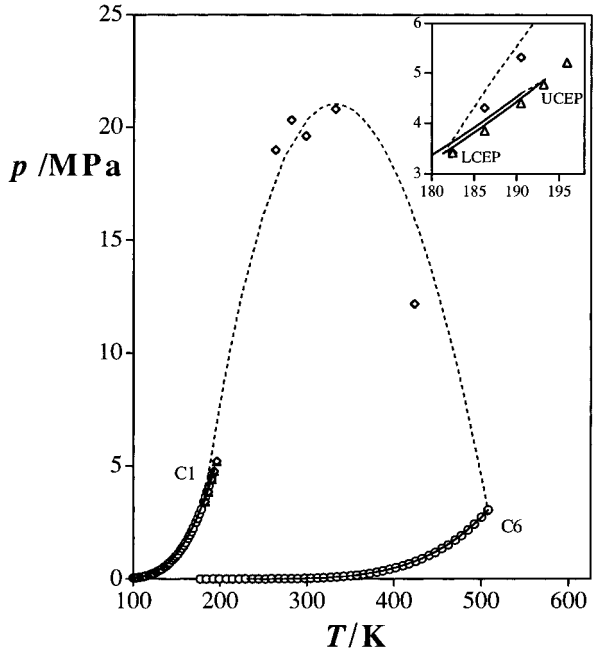

Figure 3. *pT* projection for the methane (1) + *n*-hexane (2) system compared with SAFT-VR predictions. The experimental vapor pressures for methane and *n*-hexane[30] are represented by the circles, and the critical points of the mixture are represented as diamonds.[11,28] The experimental three-phase data are represented as triangles.[11] The continuous curves represent the SAFT-VR vapor pressures of the pure components, the dashed curve corresponds to the predicted critical lines, and the short solid line, seen in the inset, is the three-phase line.

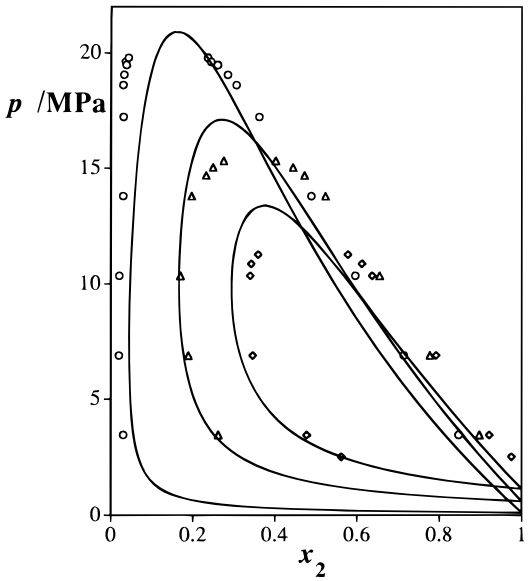

Figure 4. *px* slices at 37.78 °C (310.93 K), 137.8 °C (410.95 K), and 171.1 °C (444.25 K) (from the outer to the inner curves) for the methane (1) + *n*-hexane (2) binary mixture compared with the SAFT-VR predictions. The continuous curves represent the calculated coexistence curves and the diamonds, triangles, and circles the experimental data at 310.93, 410.95, and 444.25 K, respectively.[8]

Constant temperature *px* slices for the methane + *n*-hexane system obtained from SAFT-VR predictions are compared with experimental data[11] in Figures 4 and 5. Isotherms at 37.78 °C (310.93 K), 137.8 °C (410.95 K), and 171.1 °C (444.25 K) are shown in Figure 4, which are well above the critical point of pure methane; we observe simple gas−liquid equilibrium envelopes. The agreement between theory and experiment is good considering that we rescale the parameters of the pure components to the critical point. Five isotherms close to the

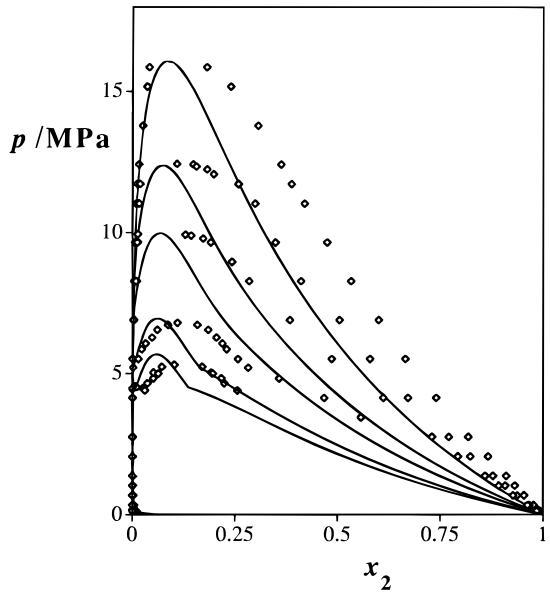

Figure 5. *px* slices at −82.65 °C (190.5 K), −77.24 °C (195.91 K), −50 °C (223.15 K), −25.01 °C (248.15 K), and 0.01 °C (273.16 K) (from the inner to the outer curves) for the methane (1) + *n*-hexane (2) binary mixture compared with the SAFT-VR predictions. The continuous curves represent the SAFT-VR prediction and the diamonds the experimental data.[11]

region of liquid−liquid immiscibility at −82.65 °C (190.5 K), −77.24 °C (195.91 K), −50 °C (223.15 K), −25.01 °C (248.15 K), and 0.01 °C (273.16 K) are presented in Figure 5. While we represent the critical pressures well, the theoretical coexistence envelopes are narrower than those observed experimentally. In the lowest temperature slice we can clearly see the region of gas−liquid coexistence, meeting the two liquid phases at the orthobaric composition. As we raise the temperature, the region of liquid−liquid immiscibility increases, this being mirrored by the experimental data. At higher temperatures still we observe the gas−liquid critical envelope, no longer seeing a liquid−liquid phase since we are now above the UCEP. We should note that at temperatures above the critical point of pure methane a gas−liquid critical point is also observed. Parameters which are not rescaled to the critical point would provide a much better description of the coexistence compositions, although the critical pressures would then be overestimated. We choose to use rescaled parameters for a better description of the critical lines.

Conclusion

The SAFT-VR approach has been used to predict the fluid-phase equilibrium of the methane + *n*-hexane binary mixture. This system shows type V phase behavior, with a region of liquid−liquid immiscibility existing over a narrow temperature range close to the critical point of pure methane. We are able to describe this region accurately using the cross interaction parameters obtained directly from the Lorentz−Berthelot mixing rules, while also achieving good agreement in the gas−liquid critical region of the phase diagram.

Dickinson et al.[31] have indicated that there is a metastable region of liquid−liquid immiscibility within the solid region of the methane + *n*-hexane phase diagram: the corresponding metastable UCST lies under the melting curve at about $T = 150$ K, $p = 1$ MPa, and $x_2 = 0.2$. The presence of a liquid−liquid critical line would mean the system would exhibit the comparatively rare type IV behavior if the solid phases are destabilized to lower temperatures. We have searched for a region of liquid−liquid immiscibility for temperatures as low

as $T = 100$ K, and the SAFT-VR theory does not predict this behavior with the Lorentz−Berthelot set of parameters.

Acknowledgment. C.M. thanks Sheffield University for a UGC scholarship, and A.G.V. thanks the Engineering and Physical Sciences Research Council (EPSRC) and the ICI Strategic Research Fund for funding Research Fellowships. We also acknowledge support from the European Commission (CI1*-CT94-0132), the Royal Society, and the Computational and ROPA Initiatives of the EPSRC for the provision of computer hardware.

References and Notes

(1) Rowlinson, J. S.; Freeman, P. I. *Pure Appl. Chem.* **1961**, *2*, 329.
(2) Kuenen, J. P.; Robson, W. G. *Phil. Mag.* **1899**, *48*, 180; *Z. Phys. Chem.* **1899**, *28*, 342.
(3) Frolich, P. K.; Tauch, E. J.; Hogan, J. J.; Peer, A. A. *J. Chem. Eng. Data* **1931**, *23*, 548.
(4) Sage, B. H.; Webster, D. C.; Lacey, W. N. *Ind. Eng. Chem.* **1936**, *28*, 1045.
(5) Boomer, E. H.; Johnson, C. A. *Can. J. Res.* **1938**, *16B*, 396.
(6) Schooch, E. P.; Hoffmann, A. E.; Mayfield, F. D. *J. Chem. Eng. Data* **1941**, *46*, 2529.
(7) Shim, J.; Kohn, J. P. *J. Chem. Eng. Data* **1962**, *7*, 3.
(8) Poston, R. S.; McKetta, J. J. *J. Chem. Eng. Data* **1966**, *11*, 362.
(9) Davenport, A. J.; Rowlinson, J. S. *Trans. Faraday Soc.* **1963**, *59*, 78.
(10) Chen, R. J. J.; Chappelear, P. S.; Kobayashi, R. *J. Chem. Eng. Data* **1976**, *21*, 213.
(11) Lin, Y.; Chen, R. J. J.; Chappelear, P. S.; Kobayashi, R. *J. Chem. Eng. Data* **1977**, *22*, 402.
(12) Scott, R. L.; van Konynenburg, P. H. *Discuss. Faraday Soc.* **1970**, *49*, 87. van Konynenburg, P. H.; Scott, R. L. *Philos. Trans. R. Soc. A* **1980**, *298*, 495.
(13) Rowlinson, J. S.; Swinton, F. L. *Liquids and Liquid Mixtures*, 3rd ed.; Butterworth Scientific: London, 1982.
(14) Chang, H. L.; Hurt, L. J.; Kobayashi, R. *AlChE. J.* **1966**, *12*, 1212.
(15) McCabe, C. M.; Galindo, A.; Gil-Villegas, A.; Jackson, G. *Int. J. Thermophys.*, in press.
(16) Gil-Villegas, A.; Galindo, A.; Whitehead, P. J.; Mills, S. J.; Jackson, G.; Burgess, A. N. *J. Chem. Phys.* **1997**, *106*, 4168.
(17) Galindo, A.; Davies, L. A.; Gil-Villegas, A.; Jackson, G. *Mol. Phys.* **1998**, *93*, 241.
(18) Chapman, W. G.; Gubbins, K. E.; Jackson, G.; Radosz, M. *Ind. Eng. Chem. Res.* **1990**, *29*, 1709. Chapman, W. G.; Gubbins, K. E.; Jackson, G.; Radosz, M. *Fluid Phase Equilib.* **1989**, *52*, 31.
(19) Galindo, A.; Whitehead, P. J.; Jackson, G.; Burgess, A. N. *J. Phys. Chem.* **1996**, *100*, 6781.
(20) Galindo, A.; Whitehead, P. J.; Jackson, G.; Burgess, A. N. *J. Phys. Chem. B* **1997**, *101*, 2082.
(21) Jackson, G.; Gubbins, K. E. *Pure Appl. Chem.* **1989**, *61*, 1021.
(22) Archer, A. L.; Amos, M. D.; Jackson, G.; McLure, I. A. *Int. J. Thermophys.* **1996**, *17*, 201.
(23) Hansen, J. P.; McDonald, I. R. *Theory of Simple Liquids*, 2nd ed.; Academic Press: New York, 1986.
(24) Leonard, P. J.; Henderson, D.; Barker, J. A. *Trans. Faraday Soc.* **1970**, *66*, 2439.
(25) Boublík, T. *J. Chem. Phys.* **1970**, *53*, 471.
(26) Mansoori, G. A.; Carnahan, N. F.; Starling, K. E.; Leland, T. W. *J. Chem. Phys.* **1971**, *54*, 1523.
(27) Carnahan, N. F.; Starling, K. E. *J. Chem. Phys.* **1969**, *51*, 635.
(28) Hicks, C. P.; Young, C. L. *Chem. Rev.* **1975**, *75*, 119.
(29) Press, W. H.; Teukolsky, S. A.; Vetterling, W. T.; Flannery, B. P. *Numerical Recipes in Fortran*, 1st ed.; Cambridge University Press: Cambridge, 1986.
(30) Smith, B. D.; Srivastava, R. *Thermodynamic Data for Pure Compounds*; Elsevier: London, 1986.
(31) Dickinson, E.; Knobler, C. M.; Scott, R. L. *J. Chem. Soc., Faraday Trans.* **1973**, *69*, 2179.